# Progranulin Deficiency in Iba-1+ Myeloid Cells Exacerbates Choroidal Neovascularization by Perturbation of Lysosomal Function and Abnormal Inflammation

**Kei Takahashi**
Gifu Pharmaceutical University
**Shinsuke Nakamura**
Gifu Pharmaceutical University
**Wataru Otsu**
Gifu Pharmaceutical University
**Masamitsu Shimazawa**
Gifu Pharmaceutical University
**Hideaki Hara** ( hidehara@gifu-pu.ac.jp )
Gifu Pharmaceutical University

**Research**

**Keywords:** progranulin, microglia, macrophage, lysosome, inflammation, neovascularization

**Posted Date:** February 9th, 2021

**DOI:** https://doi.org/10.21203/rs.3.rs-173583/v1



**Version of Record:** A version of this preprint was published at Journal of Neuroinflammation on July 25th, 2021. See the published version at https://doi.org/10.1186/s12974-021-02203-1.

For submission to *Journal of Neuroinflammation*

# Progranulin deficiency in Iba-1$^+$ myeloid cells exacerbates choroidal neovascularization by perturbation of lysosomal function and abnormal inflammation

Kei Takahashi[1], Shinsuke Nakamura[1], Wataru Otsu[2], Masamitsu Shimazawa [1,2], Hideaki Hara[1,2,*]

[1]Molecular Pharmacology, Department of Biofunctional Evaluation, Gifu Pharmaceutical University, 1-25-4 Daigaku-nishi, Gifu 501-1196, Japan.

[2]Department of Biomedical Research Laboratory, Gifu Pharmaceutical University, 1-25-4 Daigaku-nishi, Gifu 501-1196, Japan

[*]For reprints and all correspondence: H. Hara, PhD, RPh, Molecular Pharmacology, Department of Biofunctional Evaluation, Gifu Pharmaceutical University, 1-25-4 Daigaku-nishi, Gifu 501-1196, Japan.

Email: hidehara@gifu-pu.ac.jp

Short title: PGRN deficiency in Iba-1$^+$ cells exacerbates CNV

**Keywords:** progranulin, microglia, macrophage, lysosome, inflammation, neovascularization

7,281 words

# Abstract

**Background:**

Age-related macular degeneration (AMD) is the principal cause of permanent blindness among elderly individuals worldwide. Chronic inflammation in the subretinal space is associated with a progression of exudative AMD. Progranulin (PGRN) is a growth factor secreted from myeloid cells and plays an important role in controlling the lysosomal function. A deficiency of PGRN leads to inflammation of the neurons in the central nervous system. The purpose of this study was to investigate the role played by PGRN in the size of the choroidal neovascularization (CNV) in laser-induced CNV mice.

**Methods:**

CNVs were induced in C57BL/6J mice by laser photocoagulation of the retina. The expression of PGRN and the accumulation of Iba-1$^{+}$ cells around the sites of the CNVs were determined. *Grn*$^{-/-}$, *Grn*$^{+/-}$, and *Grn*$^{+/+}$ mice with laser-induced CNVs were also studied. To evaluate the effect of macrophages on the inflammation, we used a macrophage cell line (RAW264.7) in which the expression of PGRN was knocked down by RNA interference. These cells were incubated under hypoxic conditions (1% $O_2$) for 12 hours.

**Results:**

Iba-1$^+$ myeloid cells migrated and accumulated in the photocoagulation-induced CNV areas, and the CNV lesions secreted high levels of PGRN in *Grn*$^{+/+}$ mice. The size of the CNVs was larger in *Grn*$^{-/-}$ mice than in *Grn*$^{+/-}$ and *Grn*$^{+/+}$ mice. In *Grn*$^{-/-}$ mice, the number of ocular-infiltrating Iba-1$^+$ cells around the CNV was higher, and these cells produced more VEGF-A than the cells in the *Grn*$^{+/+}$ mice. PGRN-silencing of RAW264.7 cells led to an abnormal activation of the cells. In addition, hypoxic conditions promoted the production of pro-angiogenic and pro-inflammatory cytokines from PGRN-silenced macrophages. Interestingly, the expression level of lysosome-associated proteins and the number of activated lysosomes increased in siGrn-treated macrophages.

**Conclusions:**

These findings indicate that PGRN deficiency in Iba-1$^+$ cells activates the lysosomal function that then leads to abnormal inflammation. The aberrant activation of PGRN deficient Iba-1$^+$ myeloid cells might promote the progression of the CNV.

## Introduction

Age-related macular degeneration (AMD) is the principal cause of permanent blindness and visual disability among individuals over 60-years-of-age throughout the world [1]. Early AMD is usually asymptomatic even though a mottling of the retinal pigment epithelium (RPE) and extracellular drusen deposits are present between the RPE cells and Bruch's membrane [2]. Advanced AMD is subdivided into exudative and non-exudative AMD. In exudative AMD, the RPE produces excessive amounts of vascular endothelial growth factor (VEGF), and this promotes the breakdown of the blood retinal barrier and the development of choroidal neovascularization (CNV). The CNVs can penetrate Bruch's membrane and pass into the subretinal space, and the leakage of blood from these abnormal vessels can cause an acute reduction of vision [3].

Anti-VEGF therapy is the most commonly used treatment for these eyes, and it significantly suppresses the leakage from CNVs and reduces the risk of blindness [4]. While anti-VEGF therapy has improved the visual function for many patients, approximately 15% of exudative AMD patients do not respond favorably to anti-VEGF treatment [5]. Moreover, the patients who have already developed macular fibrosis or atrophy do not benefit from its use [6]. Considering these limitations of

anti-VEGF therapy, alternative strategies to treat exudative AMD are needed.

There are some evidences that chronic intraocular inflammation might be an important mechanism for the development of exudative AMD. The evidences consist of the presence of immune cells including macrophages and microglial cells in AMD lesions, and the presence of inflammatory molecules such as vitronectin, immunoglobulin, and complement proteins in drusen. In addition, there is an upregulation in the expression of different immune-related genes, such as CFH, C2/CFB, C3, CX3CR1, and TLR3/4 that are associated with the development of AMD [3][7][8]. Therefore, determining the mechanisms causing the chronic inflammation in the subretinal area might lead to new therapy for exudative AMD.

Progranulin (PGRN) is a precursor of a group of 6-kDa peptides called granulins that are commonly present in inflammatory secretions [9]. PGRN is a growth factor which is mainly found in microglial cells and neurons in the central nervous system. It plays important roles in a diverse array of biological processes such as embryonic development, cell proliferation, angiogenesis, tumorigenesis, wound repair, and inflammation [10]. Mutations in PGRN are linked to some neurodegenerative diseases including frontotemporal dementia (FTD), and to one type of lysosomal

storage disease called neuronal ceroid lipofuscinosis (NCL) [11][12]. Importantly, some studies have reported that individuals with PGRN haploinsufficiency and PGRN knockout mice (*Grn*$^{-/-}$) exhibit progressive retinal degeneration. These findings indicate that PGRN might be essential for maintaining the retinal homeostasis [13][14]. In our earlier studies, we found that PGRN plays an important role in the development and maturation of the retina [15]. Moreover, PGRN deficiency affected the number of immune cells in the developing retina [16]. However, its role in age-related eye diseases is poorly understood.

Thus, the purpose of this study was to investigate the role played by PGRN in the pathology of exudative AMD.

# Methods

## Animals

Male adult C57BL/6J mice were purchased from Japan SLC (Hamamatsu, Japan). *Grn*$^{-/-}$ mice generated by Kayasuga et al. [17] were obtained from Riken BioResource Center (Tsukuba, Japan) and were backcrossed with C57BL/6J mice. All mice were housed in an air-conditioned room maintained at 22 ± 2º C under 12:12 h light/dark cycle. The mice had free access to a standard diet (CLEA Japan) and tap water. The number of mice used for each experiment is indicated in the figure legends.

## Laser-induced choroidal neovascularization (CNV) model

The mice were anesthetized by an intramuscular injection of a mixture of ketamine (43.8 mg/kg; Daiichi Sankyo Propharma) and xylazine (2.5 mg/kg; Bayer Healthcare). The pupils were dilated with 0.5% tropicamide (Santen Pharmaceutical), and laser photocoagulation (647 nm, 120 mW, 100 ms, 50 μm; MC500, NIDEC) was performed on the right eye of each animal on day 0. Six laser spots were made around the optic disc. The endpoint of the laser burn was the appearance of a cavitation bubble which was correlated with the disruption of Bruch's membrane.

## Immunostaining of ocular sections

For immunostaining the ocular tissues, the eyes were enucleated and fixed in 4% paraformaldehyde for at least 24 h at 4º C, and then immersed in 25% sucrose in 0.01 M phosphate buffered sarin (PBS) for 2 days. The eyes were then embedded in optimal cutting temperature (OCT) compound (Sakura Finetek Japan) and immediately frozen with liquid nitrogen. Ten micrometer sections were cut with a cryostat, and the sections were mounted on glass slides (MAS COAT; Matsunami Glass).

The retinal sections were blocked in non-immune horse serum (Vector Labs) for 1 h, and then incubated with the primary antibody at 4º C overnight. The next morning the sections were covered with a secondary antibody for 1 h and then counterstained with Hoechst 33342 (1:1000; Invitrogen, catalog H3570) for 15 min.

The following antibodies were used; sheep anti-mPGRN (1:100; R&D Systems, catalog AF2557), rabbit anti-Iba1 (1:200; FUJIFILM Wako Chemicals, catalog 019-19741), Alexa Fluor® 647 donkey anti-sheep IgG (1:1000; Invitrogen, catalog A21448), and Alexa Fluor® 546 donkey anti-rabbit IgG (1:1000; Invitrogen, catalog

A10040). The immunostained sections were examined and photographed with a confocal microscope (FLUOVIEW FV10i; Olympus) or BZ-X710 (Keyence).

**Fundus fluorescein angiography (FFA)**

Two weeks after the photocoagulation (day 14), the mice were anesthetized by an intramuscular injection of ketamine and xylazine. After a dilation of the pupils and intravenous administration of 0.1 mL of a ten-fold saline dilution of 10% fluorescein (Alcon Japan), FFA was performed with a Micron IV Retinal Imaging Microscope (Phoenix Research Laboratories). The grade of leakage was assigned as described below: 1, “no leakage”, faint hyperfluorescence or mottled fluorescence; 2, “questionable leakage”, hyperfluorescent lesion without progressive increasing in intensity or size; 3, “leaky”, hyperfluorescence increasing in intensity but not in size; 4, “pathologically significant leakage”, hyperfluorexcence increasing in both intensity and size.

**Quantifications of choroidal neovascularizations**

The mice were anesthetized and were perfused with 0.5 mL PBS containing 20 mg/mL fluorescein-conjugated dextran (MW ≈ 2,000 kDa, Sigma-Aldrich). Then, their eyes were enucleated and fixed in 4% paraformaldehyde for 12 h. The cornea and

lens were removed while viewing the eye under a microscope, and the retinas were carefully peeled from the RPE-choroid-sclera complex. The RPE-choroid-sclera complexes were flat-mounted and covered with a micro cover glass (Matsunami Grass) after a few drops of fluoromount (DBS Diagnostic Biosystems) was placed on the microscope slide. The slides were viewed with BZ-X710 (Keyence) and FLUOVIEW FV10i (Olympus) microscopes. The areas of the CNV were measured using ImageJ analysis software (National Institutes of Health).

**Immunostaining of choroidal flat mounts**

The eyes for immunostaining were enucleated 7 or 14 days after photocoagulation and then fixed in 4% paraformaldehyde for 12 h. The RPE-choroid-sclera complex was separated from the retina, isolated, and blocked in non-immune horse serum (Vector Labs) for 1 h, and then incubated with the primary antibody at 4º C overnight. Then the RPE-choroid-sclera complex was stained with a secondary antibody for 1 h, and flat-mounted on the slide. The slides were viewed and photographed with the BZ-X710 (Keyence) and FLUOVIEW FV10i (Olympus) microscopes. The intensity of CD68 and VEGF-A in the CNV lesion was determined by the ImageJ analysis software (National Institutes of Health). The accumulation of Iba-1$^+$ myeloid cells around the CNV were counted in Iba-1 stained whole RPE-choroidal flat mounts

viewed from the RPE side. The primary antibodies used were: rabbit anti-Iba1 (1:200; FUJIFILM Wako Chemicals, catalog 019-19741), sheep anti-mPGRN (1:200; R&D systems, catalog AF2557), rabbit anti-VEGF-A (1:200; Merck Millipore, catalog PC315), Alexa Fluor® 647 donkey anti-sheep IgG (1:1000; Invitrogen, catalog A21448), and Alexa Fluor® 546 donkey anti-rabbit IgG (1:1000; Invitrogen, catalog A10040).

**Cell cultures**

A mouse macrophage cell line (RAW264.7) was obtained from the American Type Culture Collection (Manassas, USA). The RAW264.7 cells were grown in Dulbecco's modified Eagle's medium (DMEM; Nacalai tesque, catalog 08456-36) containing 10% fetal bovine serum (FBS) in a humidified atmosphere of 95% air and 5% $CO_2$ at 37º C. The cells were passaged by trypsinization every 2 to 3 days, and subconfluent monolayers of RAW264.7 cells from passages 10 to 16 were used in the experiments.

**Transfection by small interfering RNA and cell treatment**

To suppress the expression of PGRN in the RAW264.7 cells, three small interfering RNA (siRNA) sequences targeting *Grn* were synthesized by Invitrogen (catalog

1320001). The siRNAs (20 nmol) were transfected into RAW264.7 cells for 48 h with Lipofectamine® RNAiMAX Reagent (Invitrogen, catalog 13778-150). The sequences of the three siRNAs for PGRN were;

siRNA-a, 5'-CCAUGAUAACCAGACCUGUAAA-3',

siRNA-b, 5'-GGAACCAAGUGUUUGCGAAAGAAGA-3', and

siRNA-c, 5'-GGACCUGUGAGAAGGAUGUCGAUUU-3'.

To induce an abnormal activation of macrophages, the cell cultures were placed under hypoxic conditions. The RAW264.7 cells were incubated in 1% FBS serum containing DMEM in an oxygen-free incubator (94% $N_2$, 5% $CO_2$, 1% $O_2$) for 12 h. Control cells were incubated under normoxic conditions. After the hypoxic incubation, cell viability assay, western blotting, and immunostaining were performed. The cellular viability was determined with the Cell Counting Kit 8 (Dojindo Molecular Technologies, catalog 343-07623). For this, the cells were incubated with 10% of 2-(2-methoxy-4-nitorphenyl)-3-(4-nitrophenyl)-5-(2,4-disulfophenyl)-2H-tetrazolium, monosodium salt for 1 h at 37º C. The optical density at 450 nm was measured with a microplate reader (Varioskan Flash 2.4; Thermo Fisher Scientific).

**_In vitro_ immunostaining**

The RAW264.7 cells were fixed in 2.67% paraformaldehyde at room temperature for 30 min. The cells were then incubated with 0.2% Triton X-100 (Bio-Rad Labs, catalog #1610407) in PBS for 30 min and blocked with 1% bovine serum albumin (Nacalai tesque, catalog 01863-06) for 1 h. The cells were incubated with the primary antibodies overnight at 4º C and then incubated with secondary antibodies and Hoechst 33342 (1:1000; Invitrogen) for 1 h. The following antibodies were used; rat anti-CD68 (1:200; Bio-Rad, catalog MCA1957GA), rabbit anti-iNOS (1:200; Cell signaling technology, catalog #13120), Alexa Fluor® 488 donkey anti-rat IgG (1:1000; Invitrogen, catalog A21208), and Alexa Fluor® 546 donkey anti-rabbit IgG (1:1000; Invitrogen, catalog A10040). The images were taken with a FLUOVIEW FV10i (Olympus) fluorescent microscope.

**Western blot analysis**

For the western blot analyses, the eyes were enucleated after cervical dislocation, and the retinas and RPE-choroid-sclera complexes were isolated and rapidly frozen in liquid nitrogen. To extract the proteins, the tissue was homogenized in RIPA buffer (Sigma-Aldrich, catalog R0278) containing a protease inhibitor and a phosphatase inhibitor cocktail with a homogenizer (Microtec Co., Ltd.). In addition, the RAW264.7 cells in 24 well plates were lysed in the same buffer. The lysate was centrifuged at

12,000 g for 20 minutes, and the protein concentration was measured by comparison with known concentrations of BSA with a bicinchoninic acid protein assay kit (Pierce Chemical, catalog 23225).

The protein samples were separated on 5-20% SDS-PAGE gels, and then transferred onto a polyvinylidene difluoride membrane (Immobilon-P; Millipore, catalog IPVH00010). The following primary antibodies were used: sheep anti-mPGRN (1:200; R&D systems, catalog AF2557), rabbit anti-VEGF-A (1:200; Millipore, Catalog PC315), rabbit anti-IL-1β (1:200; abcam, catalog ab9722), mouse anti-C3 (1:200; Santa Cruz, catalog sc-28294), rabbit anti-TNF-α (1:1000; Cell Signaling Technology, catalog), rat anti-MCP-1 (1:200; Santa Cruz, catalog sc-52701), rabbit anti-sortilin (1:200; Santa Cruz, catalog sc-376561), rat anti-LAMP1 (1:500; abcam, catalog ab25245), rat anti-cathepsin D (1:500; R&D systems, catalog AF1029), and mouse anti-β-actin (1:2000; Sigma-Aldrich, catalog A2228). After exposure to the primary antibodies for at least 12 h, the membranes were incubated with horseradish peroxidase (HRP)-conjugated rabbit anti-sheep IgG, goat anti-rabbit IgG (1:2000; Thermo Scientific), goat anti-rat IgG (1:2000; Thermo Scientific), or goat anti-mouse IgG (1:2000; Thermo Scientific) for 1 h at room temperature. The immunoreactive bands were made visible with ImmunoStar LD (Wako Pure

Chemical, catalog 290-69904) and then measured with the Amersham Imager 680 blot and gel imager (GE Healthcare Life Sciences).

**Lysotracker staining**

LysoTracker Red DND-99 (LTR; Invitrogen, catalog L7528) was dissolved in PBS (50 nM) and stored at 4º C. An aliquot of the stock solutions of the dye was added to the culture media. Prior to the measurements, cells were incubated with the dye for 15 min at 37º C.

**Statistical analyses**

The data are expressed as the means ± SEMs of at least 3 independent mice, eyes, or wells. Two data sets were compared using two-tailed Welch's *t*-test. Multiple comparisons were performed using Kruskal-Wallis tests, and 1-way ANOVA followed by Tukey's or Dunnett's post hoc test. A $P$ value of $< 0.05$ was considered statistically significant. All statistical analyses were performed using SPSS (version 24.0.0.0; IBM, Armonk, NY, USA) software.

# Results

## Expression level of PGRN in eyes of CNV mouse model

To examine the pathological role of PGRN in the eye, we performed laser photocoagulation to induce the development of CNVs [18] in adult C57BL/6J mice. We examined the expression and location of PGRN and Iba-1$^+$ myeloid cells around the photocoagulated lesion by immunofluorescence staining of retinal cross-sections. The expression level of PGRN around the photocoagulated choroid was significantly higher than in normal eyes (Figure 1A). At the same time, the Iba-1$^+$ myeloid cells were found to be accumulated in the laser irradiated sites, and PGRN was seen to be located in these cells (Figure 1A and 1B). The peak of the accumulation of Iba-1$^+$ cells and PGRN$^+$Iba-1$^+$ cells in the subretinal area was 3 days after photocoagulation, and these cells remained at the lesion site even 14 days after the laser irradiation (Figure 1C, Supplemental Figure 1A).

We also determined the level of expression of PGRN in the retina and RPE-choroid-sclera complex by western blotting. While the expression level of PGRN in laser irradiated retina did not change significantly, a significant increase of PGRN was confirmed in the RPE-choroid-sclera complex at 3 and 5 days after the laser irradiation (Figures 1D, 1E).

## PGRN deficiency exacerbates vascular permeability from CNV

To examine the effects of PGRN deficiency, laser photocoagulation was performed around the optic nerve head in *Grn* WT (*Grn*$^{+/+}$), *Grn* heterozygous (*Grn*$^{+/-}$), and *Grn* deficient (*Grn*$^{-/-}$) C57BL/6J mice. Laser burns were identified in the fundus images immediately after the laser photocoagulation and 14 days after the photocoagulation. These images indicated clear differences in the size of the laser-induced scars between *Grn*$^{-/-}$, *Grn*$^{+/+}$, and *Grn*$^{+-/}$ mice at 14 days post-photocoagulation (Figure 2A). The vascular permeability was determined by fluorescein fundus angiography (FFA). Our results showed that there was no difference in fluorescein leakage between *Grn*$^{+/+}$ and *Grn*$^{+/-}$ mice; the FFA disclosed increased fluorescein leafage in *Grn*$^{-/-}$ mice compared with *Grn*$^{+/+}$ and *Grn*$^{+-/}$ mice (Figures 2A). The distribution and proportion of the lesion grades in *Grn*$^{-/-}$ mice significantly increased from those in *Grn*$^{+/+}$ and *Grn*$^{+-/}$ mice (Figures 2B). On average, the leakage grade was significantly higher in *Grn*$^{-/-}$ mice compared with *Grn*$^{+/+}$ and *Grn*$^{+-/}$ mice (Figures 2C).

## PGRN deficiency increases CNV area and number of infiltrating Iba-1$^{+}$ myeloid cells around CNVs

The size of the CNV area was also determined by FITC-dextran angiography at 14

days after the laser irradiation. Consistent with the FFA grades, the mean size of the CNV lesions was significantly larger in *Grn*$^{-/-}$ mice than in *Grn*$^{+/+}$ and *Grn*$^{+/-}$ mice. However, there was no significant difference in the size of the CNV between *Grn*$^{+/+}$ and *Grn*$^{+/-}$ mice (Figures 3A, 3B).

Infiltrating retinal microglia and systemic macrophages play an important role in the development of a CNV [19]. To determine the effects of the infiltration of Iba-1$^{+}$ myeloid cells around the CNV, immunostaining with anti-Iba-1 antibody was performed on whole RPE-choroidal flat mounts. The results showed that *Grn*$^{-/-}$ mice had significantly more Iba-1$^{+}$ cells around the CNV than *Grn*$^{+/+}$ and *Grn*$^{+/-}$ mice (Figures 3A, 3C).

**PGRN deficient macrophages have pro-angiogenic phenotype**

Seven days after the laser irradiation, the expressions of VEGF-A and CD68 were determined by immunofluorescence staining. CD68 was expressed predominantly on the lysosomal membranes of Iba-1$^{+}$ myeloid cells. The fluorescence intensity of VEGF-A in the CNV area of *Grn*$^{-/-}$ mice was higher than that in *Grn*$^{+/+}$ mice which was consistent with the intensity level of CD68$^{+}$ myeloid cells (Figures 4A, 4B, 4C).

To examine the role played by the PGRN in macrophages, we transfected small interfering RNA (siRNA) sequences targeting the PGRN in RAW264.7 cells, a mouse macrophage cell line, to silence the expression of PGRN in the cells. We first examined whether the PGRN could be silenced by the three different siRNAs targeting granulin (siGrn). Our results showed that the expression level of PGRN in RAW264.7 cells after 24-48 h transfection was higher in the scrambled siRNA (siControl) group than siGrns treated groups (Figures 4D, 4E, 4F).

Earlier studies have reported that hypoxia is one of the key inducers of CNV formation [20]. To mimic the environment around the CNV *in vitro*, PGRN silenced macrophages were incubated under hypoxic condition (1% $O_2$) for 12 h to induce abnormal activation. Compared to siControl treated cells, VEGF-A was upregulated in the siGrn cells under hypoxic conditions (Figures 4F, 4G).

**SiGrn treatment of macrophage cell line upregulates expression of inflammatory cytokines**

To examine the effects of PGRN silencing on the activation of macrophages, we determined the cell viability and expression levels of inflammatory cytokines. The cell viability of siGrn-treated RAW264.7 cells was higher than in the siControl treated

group in both the hypoxia and normoxia group (Figure 5A). When siGrn-exposed RAW264.7 cells were incubated under hypoxic conditions, several proinflammatory cytokines, viz., tumor necrosis factor-α (TNF-α), complement component 3 (C3), interleukin-1β (IL-1β), and monocyte chemotactic protein-1 (MCP-1) were increased in the siGrn- and hypoxia-treated RAW264.7 cells (Figures 5B, 5C). Moreover, the expression of inducible nitric oxide synthase (iNOS) was increased in the cells which is one of the markers of activated myeloid cells (Figure 5D).

**PGRN silenced RAW264.7 cells show lysosomal abnormality**

Lysosomal staining by a red fluorescent dye for labeling and tracking the acidic organelles (LysoTracker Red DND-99) was performed to evaluate the amount of lysosome in the PGRN-silenced macrophages. The fluorescence intensity of LysoTracker in the PGRN-silenced macrophages was significantly higher than that in the control cells (Figure 6A, 6B). In addition, the expression level of lysosomal associated membrane protein 1 (LAMP1) was higher in the siGrn- and hypoxia-treated RAW264.7 cells compared to siControl and normoxia-exposed cells (Figure 6C, 6D). Cathepsin D is a lysosomal protease which requires cleavage steps from an inactive precursor (pre-cathepsin D) to the mature state (mature-cathepsin D). In siGrn- and hypoxia-treated cells, the level of mature-cathepsin D was higher while

the level of pre-cathepsin D was lower (Figures 6C, 6E, 6F).

Sortilin is a transmembrane protein of the VPS10 family and is known to be one of the receptors for PGRN, and it mediates the delivery of PGRN into lysosomes [21]. The expression level of sortilin in siGrn-treated RAW264.7 cells was downregulated. In hypoxia exposed cells, the lower levels of sortilin was greater than in the normoxia-exposed group (Figures 6G, 6H).

## Discussion

The clinical relevance of PGRN in several autoimmune and chronic diseases, including rheumatoid arthritis, inflammatory bowel disease, diabetes mellitus, atherosclerosis, and fibrosis has been reported [22 - 26]. The loss of PGRN function can lead to the onset of several neurodegenerative diseases, e.g., FTLD and NCL, and it is accompanied by abnormal microglial activation [27]. Abnormally activated myeloid cells cause inflammatory conditions in the central nervous systems and leads to neuronal death. However, its role in chronic eye diseases is poorly understood.

Our findings demonstrated that Iba-1$^{+}$ myeloid cells including microglia and

peripheral macrophages migrate and accumulate around the CNV sites and the expression level of PGRN increase after laser photocoagulation in wild type mice (Figure 1). Moreover, 65 - 80% of Iba-1$^+$ myeloid cells around CNV lesions express PGRN (Supplemental Figure 1B). These data suggest that a significant increase of PGRN in the RPE-choroid-sclera after photocoagulation mainly caused by Iba-1$^+$ cells accumulated in CNV lesions. On the other hands, PGRN was not expressed at the laser-irradiated sites in *Grn*$^{-/-}$ mice (Supplemental Figure 2). It has been reported that PGRN promotes angiogenesis by promoting the growth and migration of the vascular endothelial cells in wound healing and tumor genesis [28][29]. In addition, it is also reported that PGRN could act as a chemoattractant to recruit microglia in brain [30]. Therefore, we originally expected that the abundant PGRN secreted from infiltrating Iba-1$^+$ myeloid cells at the lesion would promote the growth of CNVs and the accumulation of myeloid cells, resulting in exacerbation of the pathological condition. However, our results showed that the size of the CNV was significantly larger in *Grn*$^{-/-}$ mice than in *Grn*$^{+/+}$ and *Grn*$^{+/-}$ mice. Moreover, the number of ocular infiltrating Iba-1$^+$ myeloid cells around the CNVs was higher in *Grn*$^{-/-}$ mice than that in *Grn*$^{+/+}$ and *Grn*$^{+/-}$ mice (Figure 3). This difference might be due to the phenotypic changes of the Iba-1$^+$ myeloid cells associated with the PGRN deficiency. In various pathological models, the number of Iba-1$^+$ myeloid cells migrating to the lesion is

higher in PGRN-deficient mice than in wild type mice [31][32]. According to our results, PGRN might play a role in regulating the infiltration of Iba-1$^+$ myeloid cells into CNVs.

Our results also showed that myeloid cells surrounding the laser-induced injury site expressed VEGF-A (Figure 4). This indicated that myeloid cells in *Grn*$^{-/-}$ mice may have pro-angiogenic properties in the CNV lesions. VEGF-A regulates angiogenesis, enhances vascular permeability, and enhances the formation of choroidal neovascularization. In PGRN-deficient mice, the increased accumulation of myeloid cells and subsequent secretion of VEGF-A could be responsible for the development of the CNVs. Moreover, the increased VEGF-A expression from myeloid cells could also contribute to an increase of vascular permeability from the CNVs. Our results showed that the vascular permeability in *Grn*$^{-/-}$ mice was significantly higher than that in the *Grn*$^{+/+}$ and *Grn*$^{+/-}$ mice (Figure 2). These results suggest that the level of expression of pro-angiogenic factor VEGF-A from Iba-1$^+$ myeloid cells was controlled by PGRN in the inflammatory lesion. In addition, PGRN deficiency was imprecated in alteration in structure of endothelial junction and blood–brain barrier disruption [33]. Alterations in endothelial junction associated with PGRN deficiency might also contribute to the expression of the phenotypes in PGRN-deficient mice such as

increased vascular permeability and accumulation of Iba-1$^+$ myeloid cells in CNV lesions. Earlier studies have provided strong evidence that activated myeloid cells play a major role in the exacerbation of exudative AMD, e.g., myeloid cells in the CNV lesions express VEGF-A in patients with exudative AMD, and pharmacological inhibition of myeloid cell infiltration into the subretinal space significantly reduced the area of the CNV in the laser induced CNV model [19][34 - 36]. In the laser-induced CNV model, the major source of VEGF-A in the retina after the laser photocoagulation was the recruited monocytes [37]. Our results showed that most of the CD68$^+$ cells surrounding the CNVs expressed VEGF-A, and the number of Iba-1$^+$ myeloid cells was higher in *Grn*$^{-/-}$ than in *Grn*$^{+/+}$ mice (Figures 3, 4). Thus, PGRN-dependent regulation of myeloid cells might be a novel therapeutic approach to treat exudative AMD.

We also showed that silencing PGRN in RAW264.7 cells led to an abnormal activation of the cells. In addition, hypoxic conditions promoted the production of pro-angiogenic and pro-inflammatory cytokines from PGRN-silenced macrophages (Figures 4, 5). In addition to VEGF-A, various inflammatory factors including IL-1β, TNF-α, complement components, and MCP-1 have been shown to promote pathological angiogenesis directly and indirectly. [38 - 41]. Our results showed that

the levels of expression of all of these pro-inflammatory factors were significantly higher in siGrn- and hypoxia-exposed macrophages (Figure 5). Although anti-VEGF agents are commercially available to treat exudative AMD, several clinical trials have examined new therapeutic agents that target components of other signaling pathways. Therefore, a regulation of the infiltrated of Iba-1$^{+}$ myeloid cells into CNV area is important for the suppression of CNV formation, and this might be a new therapeutic method that can complement the shortcomings of anti-VEGF therapy.

In the siGrn-treated macrophages, the expression level of lysosome-associated proteins and the number of activated lysosomes were significantly higher (Figure 6). Although we did not demonstrate the mechanisms by which lysosomal activation is caused by PGRN dysfunction in this study, lysosomal abnormalities in the microglia of the brain of *Grn*$^{-/-}$ mice has been reported in recent studies. PGRN is localized to late endosomes and early lysosomes in wild type microglia, and the microglia in *Grn*$^{-/-}$ mice show a marked increase in the size and number of lysosomes [42]. Moreover, an earlier study reported that PGRN insufficiency induced lysosomal biogenesis in microglia and neurons [43][44]. Abnormal activation of lysosomal protease, such as cathepsin D and cathepsin B, results in phenotypic changes of myeloid cells through the activation of NF-κB. This activation has been shown to

induce the expression of various pro-inflammatory genes including those for cytokines and chemokines, and it also participates in inflammasome regulation [45]. Therefore, a normalization of lysosomal function in myeloid cells might be a new therapeutic target for CNV pathologies.

Next, we focused on sortilin, a transmembrane receptor, that acts as a transporter of extracellular PGRN to lysosomes rather than serving as a signaling site [46]. Interestingly, the level of expression of sortilin was significantly lower in siGrn- and hypoxia-exposed macrophages (Figure 7). The reduction of sortilin might prevent the normal transport of PGRN to lysosomes which would accelerate the abnormal activation of myeloid cells.

## Conclusion

PGRN-deficient myeloid cells have altered lysosomal function and abnormal inflammation under hypoxic stress. This leads to an exacerbation of exudative AMD (Figure 7). PGRN disfunction and lysosomal activation might play important roles in the development of exudative AMD. These findings might contribute to the development of novel anti-exudative AMD drugs.

## Ethics approval and consent to participate

All procedures used in this animal study were performed in accordance with the ARVO Statement for the Use of Animals in Ophthalmic and Vision Research, and they were approved and monitored by the Institutional Animal Care and Use Committee of Gifu Pharmaceutical University (approval nos. 2016-293, 2017-072, and 2019-195).

## Consent for publication

Not applicable.

## Availability of data and materials

Data supporting the conclusions of this article are presented in this manuscript.

## Competing interests

The authors have declared that no conflict of interest exists.

## Sources of Funding

This study was supported by grants from Nagai Memorial Research Scholarship from the Pharmaceutical Society of Japan.

## Disclosures

The authors declare that no conflict of interest exists.

## Authors' contribution

KT, SN, and HH designed all experiments. KT performed the experiments. WO and

MS helped acquire and analyze data. KT, WO, SN and HH wrote the manuscript.

**Acknowledgements**

We thank the members of our laboratory for advice and helpful discussion.

# References

1. Wong WL, Su X, Li X, Cheung CMG, Klein R, Cheng C-Y, et al. Global prevalence of age-related macular degeneration and disease burden projection for 2020 and 2040: a systematic review and meta-analysis. The Lancet Global health. 2014;2:e106-16. Available from: http://www.ncbi.nlm.nih.gov/pubmed/25104651

2. Ambati J, Atkinson JP, Gelfand BD. Immunology of age-related macular degeneration. Nature reviews Immunology. 2013;13:438–51. Available from: http://www.ncbi.nlm.nih.gov/pubmed/23702979

3. Kauppinen A, Paterno JJ, Blasiak J, Salminen A, Kaarniranta K. Inflammation and its role in age-related macular degeneration. Cellular and molecular life sciences : CMLS. 2016;73:1765–86. Available from: http://www.ncbi.nlm.nih.gov/pubmed/26852158

4. De Falco S. Antiangiogenesis therapy: an update after the first decade. The Korean journal of internal medicine. 2014;29:1–11. Available from: http://www.ncbi.nlm.nih.gov/pubmed/24574826

5. Krebs I, Glittenberg C, Ansari-Shahrezaei S, Hagen S, Steiner I, Binder S. Non-responders to treatment with antagonists of vascular endothelial growth factor in age-related macular degeneration. The British journal of ophthalmology. 2013;97:1443–6. Available from: http://www.ncbi.nlm.nih.gov/pubmed/23966368

6. Little K, Ma JH, Yang N, Chen M, Xu H. Myofibroblasts in macular fibrosis secondary to neovascular age-related macular degeneration - the potential sources and molecular cues for their recruitment and activation. EBioMedicine. 2018;38:283–91. Available from: http://www.ncbi.nlm.nih.gov/pubmed/30473378

7. Chen M, Xu H. Parainflammation, chronic inflammation, and age-related macular degeneration. Journal of leukocyte biology. 2015;98:713–25. Available from: http://www.ncbi.nlm.nih.gov/pubmed/26292978

8. Anderson DH, Mullins RF, Hageman GS, Johnson L V. A role for local inflammation in the formation of drusen in the aging eye. American journal of ophthalmology. 2002;134:411–31. Available from: http://www.ncbi.nlm.nih.gov/pubmed/12208254

9. Hrabal R, Chen Z, James S, Bennett HP, Ni F. The hairpin stack fold, a novel protein architecture for a new family of protein growth factors. Nature structural biology. 1996;3:747–52. Available from: http://www.ncbi.nlm.nih.gov/pubmed/8784346

10. Bateman A, Bennett HPJ. The granulin gene family: from cancer to dementia. BioEssays : news and reviews in molecular, cellular and developmental biology. 2009;31:1245–54. Available from: http://www.ncbi.nlm.nih.gov/pubmed/19795409

11. Baker M, Mackenzie IR, Pickering-Brown SM, Gass J, Rademakers R, Lindholm

C, et al. Mutations in progranulin cause tau-negative frontotemporal dementia linked to chromosome 17. Nature. 2006;442:916–9. Available from: http://www.ncbi.nlm.nih.gov/pubmed/16862116

12. Canafoglia L, Morbin M, Scaioli V, Pareyson D, D'Incerti L, Fugnanesi V, et al. Recurrent generalized seizures, visual loss, and palinopsia as phenotypic features of neuronal ceroid lipofuscinosis due to progranulin gene mutation. Epilepsia. 2014;55:e56-9. Available from: http://www.ncbi.nlm.nih.gov/pubmed/24779634

13. Hafler BP, Klein ZA, Jimmy Zhou Z, Strittmatter SM. Progressive retinal degeneration and accumulation of autofluorescent lipopigments in Progranulin deficient mice. Brain research. 2014;1588:168–74. Available from: http://www.ncbi.nlm.nih.gov/pubmed/25234724

14. Ward ME, Chen R, Huang H-Y, Ludwig C, Telpoukhovskaia M, Taubes A, et al. Individuals with progranulin haploinsufficiency exhibit features of neuronal ceroid lipofuscinosis. Science translational medicine. 2017;9. Available from: http://www.ncbi.nlm.nih.gov/pubmed/28404863

15. Kuse Y, Tsuruma K, Mizoguchi T, Shimazawa M, Hara H. Progranulin deficiency causes the retinal ganglion cell loss during development. Scientific reports. 2017;7:1679. Available from: http://www.ncbi.nlm.nih.gov/pubmed/28490764

16. Kuse Y, Ohuchi K, Nakamura S, Hara H, Shimazawa M. Microglia increases the

proliferation of retinal precursor cells during postnatal development. Molecular vision. 2018;24:536–45. Available from: http://www.ncbi.nlm.nih.gov/pubmed/30090016

17. Kayasuga Y, Chiba S, Suzuki M, Kikusui T, Matsuwaki T, Yamanouchi K, et al. Alteration of behavioural phenotype in mice by targeted disruption of the progranulin gene. Behavioural brain research. 2007;185:110–8. Available from: http://www.ncbi.nlm.nih.gov/pubmed/17764761

18. Lambert V, Lecomte J, Hansen S, Blacher S, Gonzalez M-LA, Struman I, et al. Laser-induced choroidal neovascularization model to study age-related macular degeneration in mice. Nature protocols. 2013;8:2197–211. Available from: http://www.ncbi.nlm.nih.gov/pubmed/24136346

19. Xu N, Bo Q, Shao R, Liang J, Zhai Y, Yang S, et al. Chitinase-3-Like-1 Promotes M2 Macrophage Differentiation and Induces Choroidal Neovascularization in Neovascular Age-Related Macular Degeneration. Investigative ophthalmology & visual science. 2019;60:4596–605. Available from: http://www.ncbi.nlm.nih.gov/pubmed/31675076

20. Takata S, Masuda T, Nakamura S, Kuchimaru T, Tsuruma K, Shimazawa M, et al. The effect of triamcinolone acetonide on laser-induced choroidal neovascularization in mice using a hypoxia visualization bio-imaging probe. Scientific reports. 2015;5:9898. Available from: http://www.ncbi.nlm.nih.gov/pubmed/25927172

21. Hu F, Padukkavidana T, Vægter CB, Brady OA, Zheng Y, Mackenzie IR, et al. Sortilin-mediated endocytosis determines levels of the frontotemporal dementia protein, progranulin. Neuron. 2010;68:654–67. Available from: http://www.ncbi.nlm.nih.gov/pubmed/21092856

22. Cerezo LA, Kuklová M, Hulejová H, Vernerová Z, Kaspříková N, Veigl D, et al. Progranulin Is Associated with Disease Activity in Patients with Rheumatoid Arthritis. Mediators of inflammation. 2015;2015:740357. Available from: http://www.ncbi.nlm.nih.gov/pubmed/26339140

23. Thurner L, Stöger E, Fadle N, Klemm P, Regitz E, Kemele M, et al. Proinflammatory progranulin antibodies in inflammatory bowel diseases. Digestive diseases and sciences. 2014;59:1733–42. Available from: http://www.ncbi.nlm.nih.gov/pubmed/24591016

24. Youn B-S, Bang S-I, Klöting N, Park JW, Lee N, Oh J-E, et al. Serum progranulin concentrations may be associated with macrophage infiltration into omental adipose tissue. Diabetes. 2009;58:627–36. Available from: http://www.ncbi.nlm.nih.gov/pubmed/19056610

25. Kojima Y, Ono K, Inoue K, Takagi Y, Kikuta K, Nishimura M, et al. Progranulin expression in advanced human atherosclerotic plaque. Atherosclerosis. 2009;206:102–8. Available from: http://www.ncbi.nlm.nih.gov/pubmed/19321167

26. Yilmaz Y, Eren F, Yonal O, Polat Z, Bacha M, Kurt R, et al. Serum progranulin as an independent marker of liver fibrosis in patients with biopsy-proven nonalcoholic fatty liver disease. Disease markers. 2011;31:205–10. Available from: http://www.ncbi.nlm.nih.gov/pubmed/22045426

27. Mendsaikhan A, Tooyama I, Walker DG. Microglial Progranulin: Involvement in Alzheimer's Disease and Neurodegenerative Diseases. Cells. 2019;8. Available from: http://www.ncbi.nlm.nih.gov/pubmed/30862089

28. He Z, Ong CHP, Halper J, Bateman A. Progranulin is a mediator of the wound response. Nature medicine. 2003;9:225–9. Available from: http://www.ncbi.nlm.nih.gov/pubmed/12524533

29. Eguchi R, Nakano T, Wakabayashi I. Progranulin and granulin-like protein as novel VEGF-independent angiogenic factors derived from human mesothelioma cells. Oncogene. 2017;36:714–22. Available from: http://www.ncbi.nlm.nih.gov/pubmed/27345409

30. Pickford F, Marcus J, Camargo LM, Xiao Q, Graham D, Mo J-R, et al. Progranulin Is a Chemoattractant for Microglia and Stimulates Their Endocytic Activity. The American Journal of Pathology. 2011;178:284–95. Available from: https://linkinghub.elsevier.com/retrieve/pii/S0002944010000489

31. Sugihara H, Miyaji K, Yamanouchi K, Matsuwaki T, Nishihara M. Progranulin

deficiency leads to prolonged persistence of macrophages, accompanied with myofiber hypertrophy in regenerating muscle. The Journal of veterinary medical science. 2018;80:346–53. Available from: http://www.ncbi.nlm.nih.gov/pubmed/29249750

32. Yu Y, Xu X, Liu L, Mao S, Feng T, Lu Y, et al. Progranulin deficiency leads to severe inflammation, lung injury and cell death in a mouse model of endotoxic shock. Journal of cellular and molecular medicine. 2016;20:506–17. Available from: http://www.ncbi.nlm.nih.gov/pubmed/26757107

33. Jackman K, Kahles T, Lane D, Garcia-Bonilla L, Abe T, Capone C, et al. Progranulin deficiency promotes post-ischemic blood-brain barrier disruption. The Journal of neuroscience : the official journal of the Society for Neuroscience. 2013;33:19579–89. Available from: http://www.ncbi.nlm.nih.gov/pubmed/24336722

34. Grossniklaus HE, Miskala PH, Green WR, Bressler SB, Hawkins BS, Toth C, et al. Histopathologic and ultrastructural features of surgically excised subfoveal choroidal neovascular lesions: submacular surgery trials report no. 7. Archives of ophthalmology (Chicago, Ill : 1960). 2005;123:914–21. Available from: http://www.ncbi.nlm.nih.gov/pubmed/16009831

35. Espinosa-Heidmann DG, Suner IJ, Hernandez EP, Monroy D, Csaky KG, Cousins SW. Macrophage depletion diminishes lesion size and severity in

1 experimental choroidal neovascularization. Investigative ophthalmology & visual
2 science. 2003;44:3586–92. Available from:
3 http://www.ncbi.nlm.nih.gov/pubmed/12882811
4 36. Crespo-Garcia S, Corkhill C, Roubeix C, Davids A-M, Kociok N, Strauss O, et al.
5 Inhibition of Placenta Growth Factor Reduces Subretinal Mononuclear Phagocyte
6 Accumulation in Choroidal Neovascularization. Investigative ophthalmology & visual
7 science. 2017;58:4997–5006. Available from:
8 http://www.ncbi.nlm.nih.gov/pubmed/28979997
9 37. Itaya M, Sakurai E, Nozaki M, Yamada K, Yamasaki S, Asai K, et al.
10 Upregulation of VEGF in murine retina via monocyte recruitment after retinal scatter
11 laser photocoagulation. Investigative ophthalmology & visual science.
12 2007;48:5677–83. Available from: http://www.ncbi.nlm.nih.gov/pubmed/18055819
13 38. Lavalette S, Raoul W, Houssier M, Camelo S, Levy O, Calippe B, et al.
14 Interleukin-1β inhibition prevents choroidal neovascularization and does not
15 exacerbate photoreceptor degeneration. The American journal of pathology.
16 2011;178:2416–23. Available from: http://www.ncbi.nlm.nih.gov/pubmed/21514452
17 39. Wang H, Han X, Wittchen ES, Hartnett ME. TNF-α mediates choroidal
18 neovascularization by upregulating VEGF expression in RPE through ROS-
19 dependent β-catenin activation. Molecular vision. 2016;22:116–28. Available from:

http://www.ncbi.nlm.nih.gov/pubmed/26900328

40. Long Q, Cao X, Bian A, Li Y. C3a Increases VEGF and Decreases PEDF mRNA Levels in Human Retinal Pigment Epithelial Cells. BioMed research international. 2016;2016:6958752. Available from: http://www.ncbi.nlm.nih.gov/pubmed/27747237

41. Lechner J, Chen M, Hogg RE, Toth L, Silvestri G, Chakravarthy U, et al. Peripheral blood mononuclear cells from neovascular age-related macular degeneration patients produce higher levels of chemokines CCL2 (MCP-1) and CXCL8 (IL-8). Journal of neuroinflammation. 2017;14:42. Available from: http://www.ncbi.nlm.nih.gov/pubmed/28231837

42. Lui H, Zhang J, Makinson SR, Cahill MK, Kelley KW, Huang H-Y, et al. Progranulin Deficiency Promotes Circuit-Specific Synaptic Pruning by Microglia via Complement Activation. Cell. 2016;165:921–35. Available from: http://www.ncbi.nlm.nih.gov/pubmed/27114033

43. Tanaka Y, Matsuwaki T, Yamanouchi K, Nishihara M. Increased lysosomal biogenesis in activated microglia and exacerbated neuronal damage after traumatic brain injury in progranulin-deficient mice. Neuroscience. 2013;250:8–19. Available from: http://www.ncbi.nlm.nih.gov/pubmed/23830905

44. Tanaka Y, Suzuki G, Matsuwaki T, Hosokawa M, Serrano G, Beach TG, et al. Progranulin regulates lysosomal function and biogenesis through acidification of

lysosomes. Human molecular genetics. 2017;26:969–88. Available from: http://www.ncbi.nlm.nih.gov/pubmed/28073925

45. Ni J, Wu Z, Peterts C, Yamamoto K, Qing H, Nakanishi H. The Critical Role of Proteolytic Relay through Cathepsins B and E in the Phenotypic Change of Microglia/Macrophage. The Journal of neuroscience : the official journal of the Society for Neuroscience. 2015;35:12488–501. Available from: http://www.ncbi.nlm.nih.gov/pubmed/26354916

46. Kao AW, McKay A, Singh PP, Brunet A, Huang EJ. Progranulin, lysosomal regulation and neurodegenerative disease. Nature reviews Neuroscience. 2017;18:325–33. Available from: http://www.ncbi.nlm.nih.gov/pubmed/28435163

# Figure legends

**Figure 1. Expression level of progranulin in eyes of a choroidal neovascularization (CNV) model mouse**

A. Immunofluorescence staining of a laser-injured eye of a C57BL/6J mice (8-weeks-old) at 0, 1, 3, 5, 7, and 14 days after the photocoagulation with anti-PGRN (green) and anti-Iba-1 (red) antibodies. Nuclei were stained with Hoechst 33342 (blue). Phase contrast images are also shown. Scale bar: 50 μm.

B. Enlarged images at 3 days after laser irradiation. Scale bar: 10 μm.

C. Quantitative analysis of the number of $PGRN^+$ $Iba\text{-}1^+$ cells in subretinal area after laser irradiation.

D. and E. PGRN expression levels in the retina and RPE-choroid-sclera from C57BL/6J mice at 0, 1, 3, 5, and 7 days after photocoagulation. Data are the means ± SEMs, (n = 5). $^{*}P$ <0.05, $^{**}P$ <0.01 vs. Control (one-way ANOVA followed by Dunnett's test).

**Figure 2. Increased vascular leakage from CNV in progranulin knockout mice**

A. Representative photographs of ocular fundus from $Grn^{+/+}$, $Grn^{+/-}$, and $Grn^{-/-}$ mice (9-12 weeks) immediately after laser irradiation. Angiographic images at 14 days after photocoagulation.

B. Graph of the FFA grade scores of each laser spots (*Grn*$^{+/+}$, 64 laser spots; *Grn*$^{+/-}$, 75 laser spots; and *Grn*$^{-/-}$, 57 laser spots). Data are presented as percentages. $^{*}P$ <0.05 vs. *Grn*$^{+/+}$, $^{\#}P$ <0.05 vs. *Grn*$^{+/-}$ (Kruskal-Walis test).

C. Graph of the average leakage grade. (*Grn*$^{+/+}$, n = 11; *Grn*$^{+/}$, n = 13; and *Grn*$^{-/-}$, n = 10). Data are the means ± SEMs. $^{*}P$ <0.05, vs. *Grn*$^{+/+}$; $^{\#}P$ <0.05, vs. *Grn*$^{+/-}$ (one-way ANOVA followed by Tukey's test)

**Figure 3. Larger size laser-induced CNV lesion and higher number of Iba-1$^{+}$ cells in the progranulin knockout mice**

A. Representative microscopic images of FITC-dextran angiogram and immunostaining of Iba-1 of RPE-choroid flat mounts from *Grn*$^{+/+}$, *Grn*$^{+/-}$ and *Grn*$^{-/-}$ mice (9-12 weeks). White dotted line shows CNV area. Scale bars: 50 μm.

B. Quantification of the mean size of the CNV areas.

C. Quantification of the number of Iba-1$^{+}$ cells around the CNVs (*Grn*$^{+/+}$, n = 9; *Grn*$^{+/}$, n = 14; and *Grn*$^{-/-}$, n = 10). Data are the means ± SEMs. $^{*}P$ <0.05, $^{**}P$ <0.01 vs. *Grn*$^{+/+}$; $^{\#}P$ <0.05, $^{\#\#}P$ <0.01 vs. *Grn*$^{+/-}$ (one-way ANOVA followed by Tukey's test).

**Figure 4. Pro-angiogenic phenotype of progranulin deficient macrophages**

A. Immunofluorescent staining of laser-irradiated RPE-choroid complex from *Grn*$^{+/+}$

and *Grn*$^{-/-}$ mice (9-12 weeks) with anti-VEGF-A (white) and anti-CD68 (red) antibodies. Nuclei and CNV are stained with Hoechst 33342 (blue) and FITC-dextran (green). White dotted line shows CNV area. Scale bars, 50 μm.

B. and C. Quantification of gray value of VEGF-A (B) and CD68 (C) in CNV area (*Grn*$^{+/+}$, n = 3; and *Grn*$^{-/-}$, n = 4). Data are the means ± SEMs. $^{*}P < 0.05$ vs. *Grn*$^{+/+}$ Welch's *t*-test).

D. and E. PGRN expression level in RAW264.7 cells after transfection with siControl or three types of siGrns (n = 4).

F. and G. PGRN and VEGF-A expression levels in RAW264.7 cells after transfection by siControl or siGrn#1 and exposure to hypoxia. Data are the means ± SEMs (n = 4). $^{*}P$ <0.05; $^{**}P$ <0.01 vs. siControl; $^{\#}P$ <0.05; $^{\#\#}P$ <0.01 vs. siControl+Hypoxia (one-way ANOVA followed by Tukey's tests).

**Figure 5. Higher levels of pro-inflammatory cytokines in progranulin silenced RAW264.7 cells**

A. Cell viability of RAW264.7 cells after transfection in siControl or siGrn mice and exposure to hypoxia. Data are the means ± SEMs (n = 6). $^{*}P$ <0.05 vs. siControl; $^{\#\#}P$ <0.01 vs. siControl + Hypoxia (Welch's *t*-test)

B. Representative western blots showing immunoreactivity against TNF-α, C3, IL-1β,

MCP-1, and β-actin.

C. Quantitative analysis of expression level of TNF-α, C3, IL-1β, and MCP-1 in RAW264.7 cells. Data are the means ± SEMs (n = 4). $^{*}P$ <0.05; $^{**}P$ <0.01 vs. siControl; $^{\#}P$ <0.05, $^{\#\#}P$ <0.01 vs. siControl + Hypoxia (one-way ANOVA followed by Tukey's tests).

D. Immunofluorescence staining of RAW264.7 cells with anti-iNOS (green) and anti-CD68 (red) antibodies. Nuclei were stained with Hoechst 33342 (blue). Scale bar: 10 μm.

**Figure 6. Lysosomal abnormality in progranulin-silenced macrophages**

A. Representative images of LysoTracker Red DND-99 staining (red) and phase contrast images of RAW264.7 cells after transfection by siControl or siGrn. Scale bar: 10 μm.

B. Quantitative analysis of the fluorescence intensity of LysoTracker$^{+}$ cells. Data are the means ± SEM (n = 6). *$P$ <0.05 vs. siControl (Welch's *t*-test).

C. Representative images of western blots showing immunoreactivity against LAMP1, cathepsin D, and β-actin.

D. E. and F. Quantitative analysis of expression level of LAMP1 (D), pre-cathepsin D (E), and mature-cathepsin D (F) in RAW264.7 cells after transfection of siControl or

siGrn and exposure to hypoxia (1% $O_2$, 12 h).

G. and H. Level of expression of sortilin in RAW264.7 cells after transfection by siControl or siGrn and exposure to hypoxia. Data are the means ± SEMs (n = 4). $^{*}P$ <0.05; $^{**}P$ <0.01 vs. siControl; $^{\#}P$ <0.05; $^{\#\#}P$ <0.01 vs. siControl + Hypoxia (one-way ANOVA followed by Tukey's tests).

**Figure 7. Graphical abstract**

In wild type mice, the myeloid cells including the microglia and macrophages express high levels of PGRN in response to acute inflammation. PGRN regulates the lysosomal function and activation in myeloid cells. However, in PGRN deficient mice, the reduced levels of PGRN lead to abnormal activation of the lysosomes in the myeloid cells. Lysosome activated myeloid cells express proangiogenic and proinflammatory factors and promote formation of CNV and vascular permeability.

**Supplemental Figure 1. The accumulation of Iba-1$^{+}$ cells in subretinal area after laser irradiation and the expression of PGRN in Iba-1$^{+}$ cells.**

A. Quantitative analysis of the number of Iba-1$^{+}$ cells in subretinal area after laser irradiation. The peak of the accumulation of Iba-1$^{+}$ cells in the subretinal area was 3 days after photocoagulation, and these cells remained at the lesion site even 14

days after the laser irradiation. Data are the means ± SEMs, (n = 5). $^{*}P$ <0.05, $^{**}P$ <0.01 vs. Control (one-way ANOVA followed by Dunnett's test).

B. Graph of the ratio of $PGRN^{+}$ cells in $Iba\text{-}1^{+}$ cells around CNVs. Data are presented as percentages. Expression of PGRN was observed in 65-80% of $iba\text{-}1^{+}$ cells in CNV lesions.

**Supplemental Figure 2. Progranulin expression in CNV lesion in WT and KO mice**

A. Immunofluorescent staining of CNV lesion from $Grn^{+/+}$ and $Grn^{-/-}$ mice with anti-PGRN (magenta) antibodies. PGRN was not expressed at the laser-irradiated sites in $Grn^{-/-}$ mice. Nuclei and CNV are stained with Hoechst 33342 (blue) and FITC-dextran (green). Scale bars, 50 μm.

# Figures

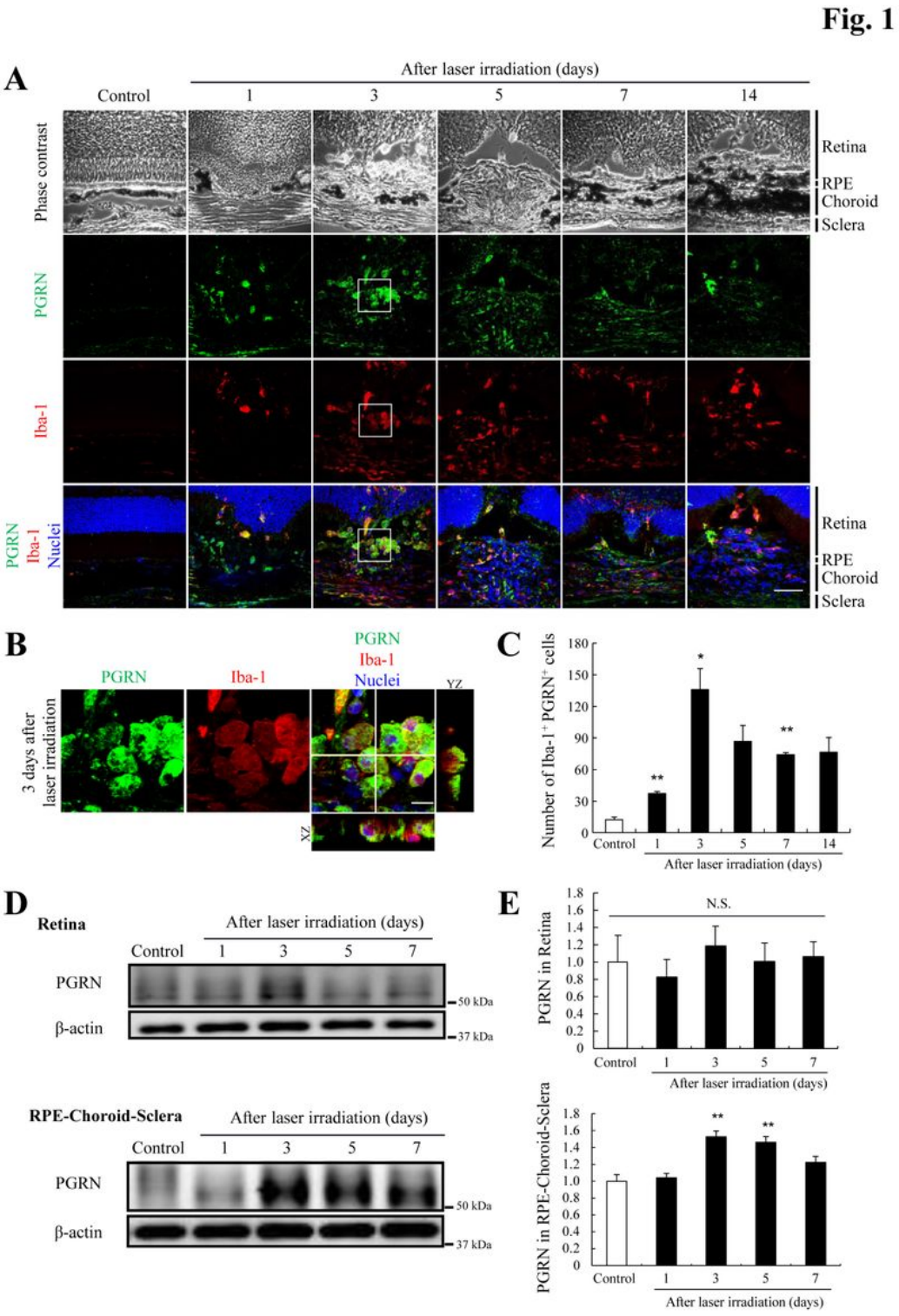


## Figure 1

Expression level of progranulin in eyes of a choroidal neovascularization (CNV) model mouse A. Immunofluorescence staining of a laser-injured eye of a C57BL/6J mice (8-weeks-old) at 0, 1, 3, 5, 7, and 14 days after the photocoagulation with anti-PGRN (green) and anti-Iba-1 (red) antibodies. Nuclei were

stained with Hoechst 33342 (blue). Phase contrast images are also shown. Scale bar: 50 μm. B. Enlarged images at 3 days after laser irradiation. Scale bar: 10 μm. C. Quantitative analysis of the number of PGRN+ Iba-1+ cells in subretinal area after laser irradiation. D. and E. PGRN expression levels in the retina and RPE-choroid-sclera from C57BL/6J mice at 0, 1, 3, 5, and 7 days after photocoagulation. Data are the means ± SEMs, (n = 5). *P <0.05, **P <0.01 vs. Control (one-way ANOVA followed by Dunnett's test).

**Fig. 2**

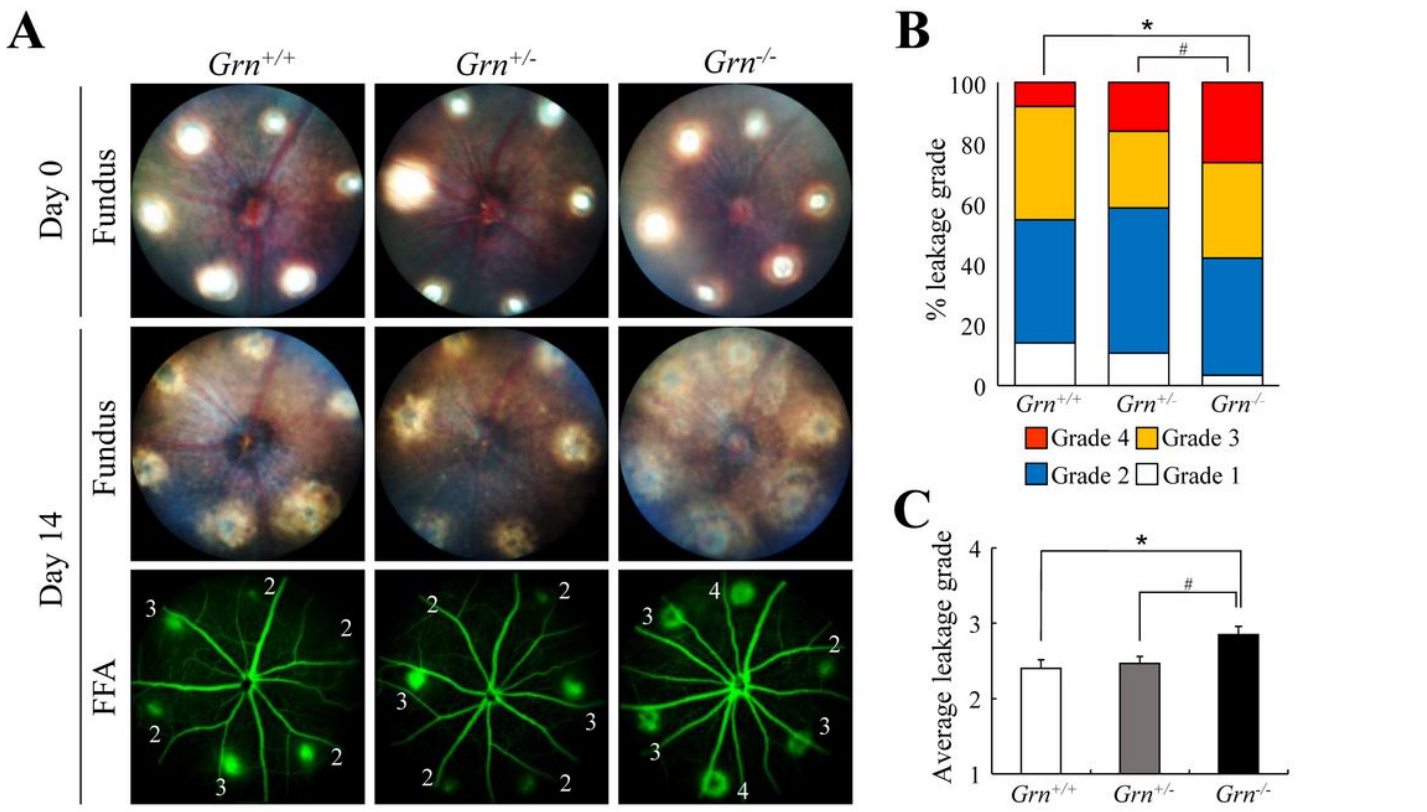


## Figure 2

Increased vascular leakage from CNV in progranulin knockout mice A. Representative photographs of ocular fundus from Grn+/+, Grn+/-, and Grn-/- mice (9-12 weeks) immediately after laser irradiation. Angiographic images at 14 days after photocoagulation. B. Graph of the FFA grade scores of each laser spots (Grn+/+, 64 laser spots; Grn+/-, 75 laser spots; and Grn-/-, 57 laser spots). Data are presented as percentages. *P <0.05 vs. Grn+/+, #P <0.05 vs. Grn+/- (Kruskal-Walis test). C. Graph of the average leakage grade. (Grn+/+, n = 11; Grn+/, n = 13; and Grn-/-, n = 10). Data are the means ± SEMs. *P <0.05, vs. Grn+/+; #P <0.05, vs. Grn+/- (one-way ANOVA followed by Tukey's test)

Fig. 3

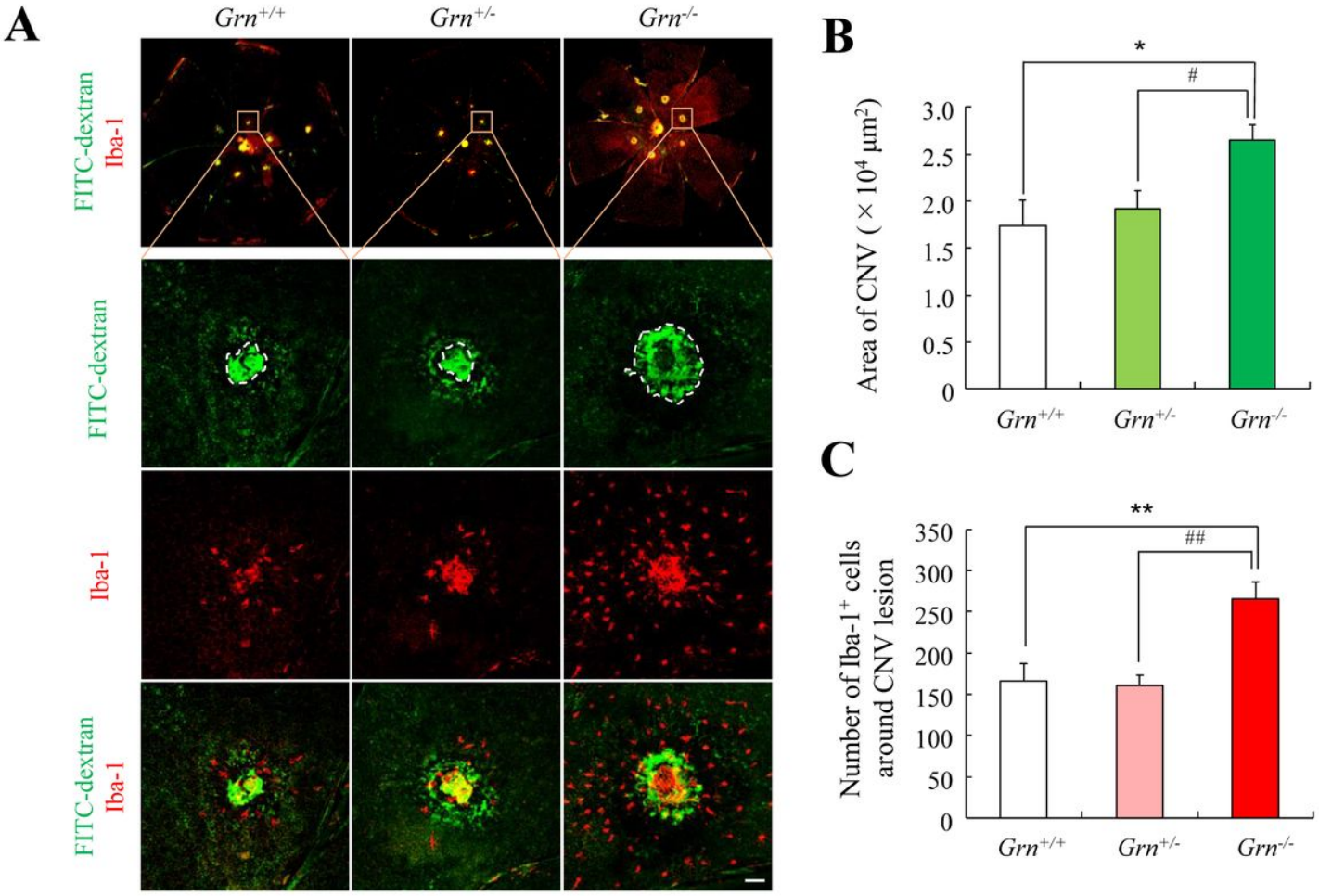


## Figure 3

Larger size laser-induced CNV lesion and higher number of Iba-1+ cells in the progranulin knockout mice A. Representative microscopic images of FITC-dextran angiogram and immunostaining of Iba-1 of RPE-choroid flat mounts from Grn+/+, Grn+/- and Grn-/- mice (9-12 weeks). White dotted line shows CNV area. Scale bars: 50 μm. B. Quantification of the mean size of the CNV areas. C. Quantification of the number of Iba-1+ cells around the CNVs (Grn+/+, n = 9; Grn+/, n = 14; and Grn-/-, n = 10). Data are the means ± SEMs. *P <0.05, **P <0.01 vs. Grn+/+; #P <0.05, ##P <0.01 vs. Grn+/- (one-way ANOVA followed by Tukey's test).

Fig. 4

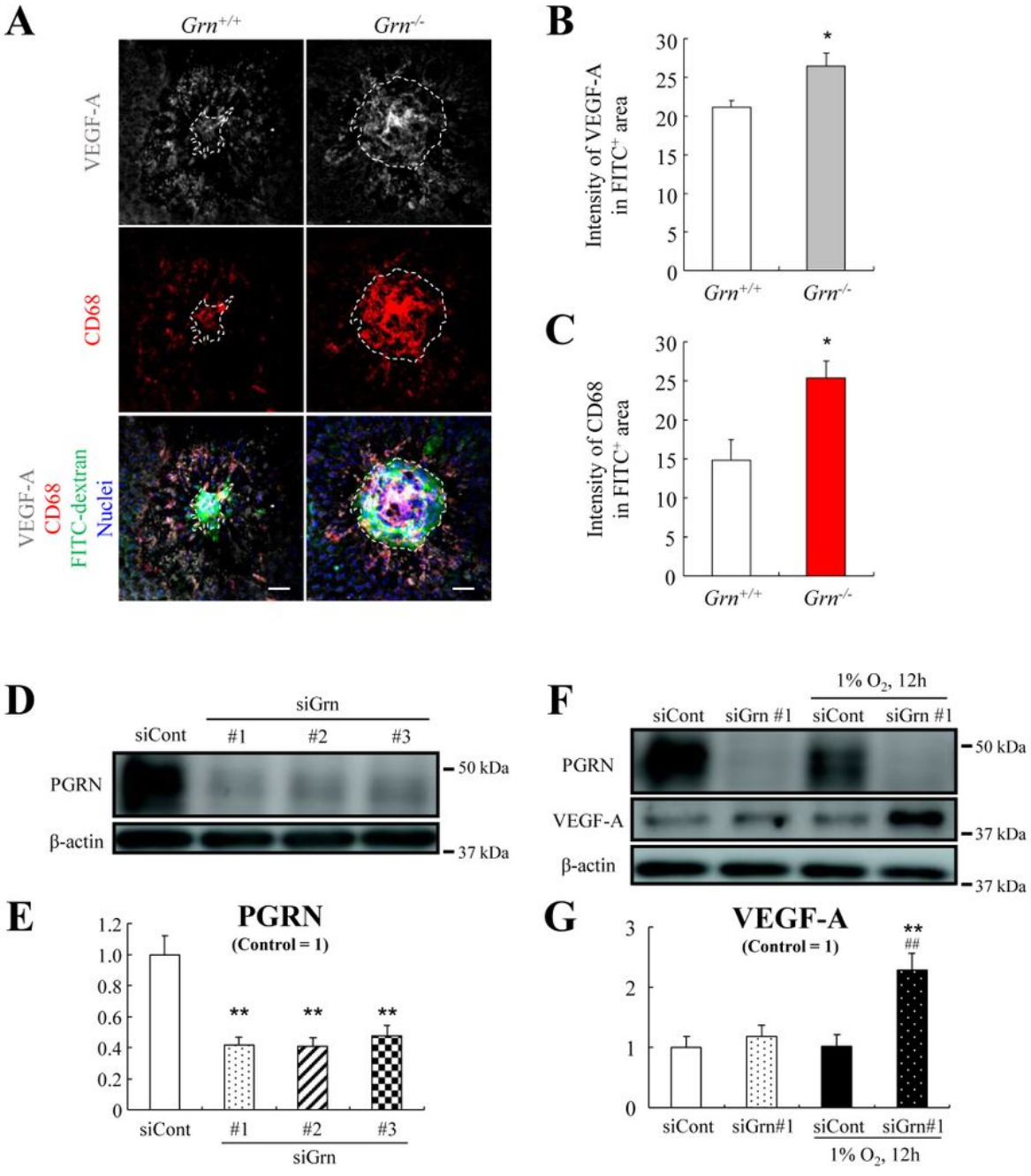


## Figure 4

Pro-angiogenic phenotype of progranulin deficient macrophages A. Immunofluorescent staining of laser-irradiated RPE-choroid complex from Grn+/+ and Grn-/- mice (9-12 weeks) with anti-VEGF-A (white) and anti-CD68 (red) antibodies. Nuclei and CNV are stained with Hoechst 33342 (blue) and FITC-dextran (green). White dotted line shows CNV area. Scale bars, 50 μm. B. and C. Quantification of gray value of VEGF-A (B) and CD68 (C) in CNV area (Grn+/+, n = 3; and Grn-/-, n = 4). Data are the means ± SEMs. *P <

0.05 vs. Grn+/+ Welch's t-test). D. and E. PGRN expression level in RAW264.7 cells after transfection with siControl or three types of siGrns (n = 4). F. and G. PGRN and VEGF-A expression levels in RAW264.7 cells after transfection by siControl or siGrn#1 and exposure to hypoxia. Data are the means ± SEMs (n = 4). *P <0.05; **P <0.01 vs. siControl; #P <0.05; ##P <0.01 vs. siControl+Hypoxia (one-way ANOVA followed by Tukey's tests).

**Fig. 5**

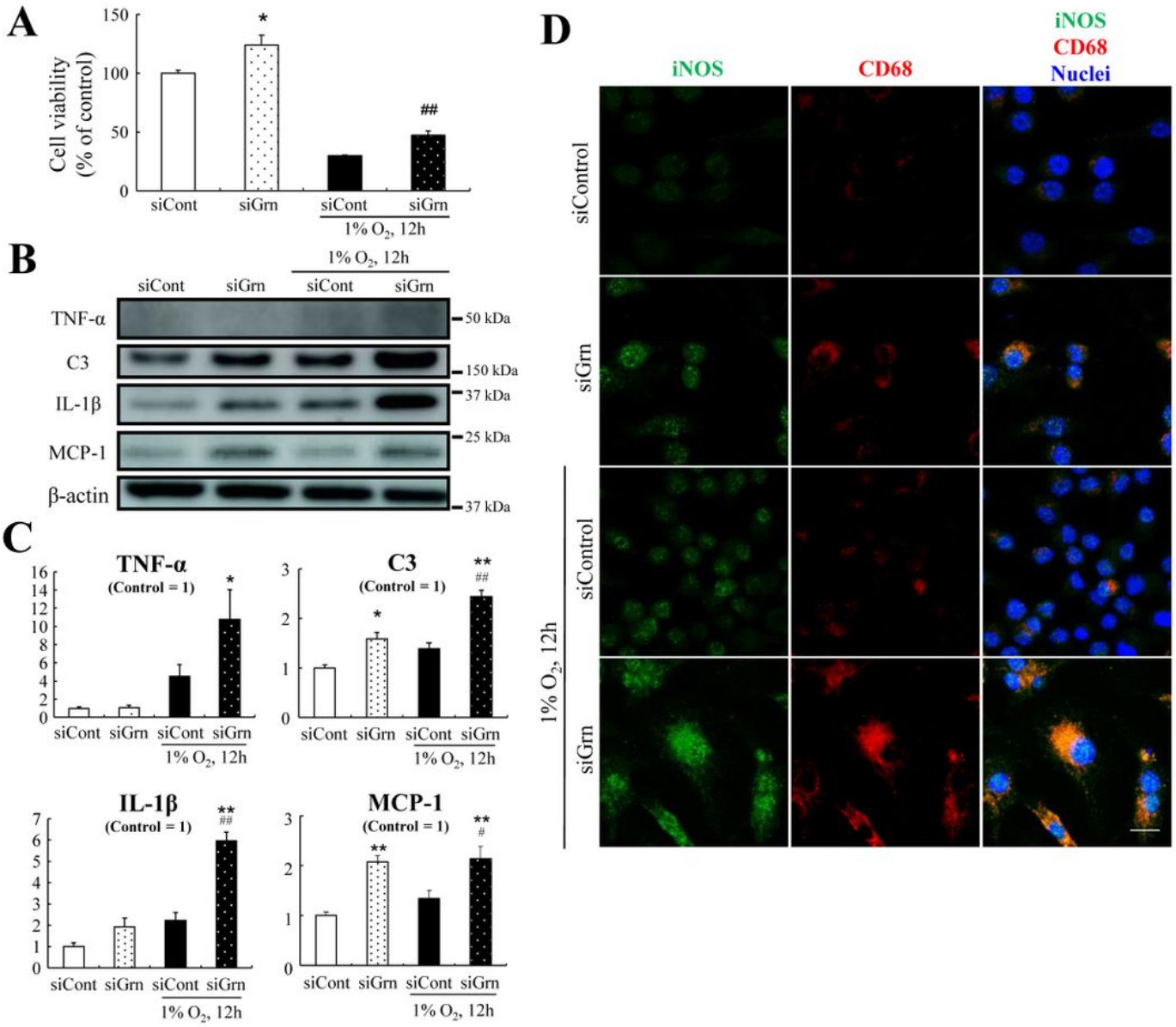


Figure 5

Higher levels of pro-inflammatory cytokines in progranulin silenced RAW264.7 cells A. Cell viability of RAW264.7 cells after transfection in siControl or siGrn mice and exposure to hypoxia. Data are the means ± SEMs (n = 6). *P <0.05 vs. siControl; ##P <0.01 vs. siControl + Hypoxia (Welch's t-test) B. Representative western blots showing immunoreactivity against TNF-α, C3, IL-1β, MCP-1, and β-actin. C. Quantitative analysis of expression level of TNF-α, C3, IL-1β, and MCP-1 in RAW264.7 cells. Data are the means ± SEMs (n = 4). *P <0.05; **P <0.01 vs. siControl; #P <0.05, ##P <0.01 vs. siControl + Hypoxia (one-way ANOVA followed by Tukey's tests). D. Immunofluorescence staining of RAW264.7 cells with anti-iNOS (green) and anti-CD68 (red) antibodies. Nuclei were stained with Hoechst 33342 (blue). Scale bar: 10 μm.

Fig. 6

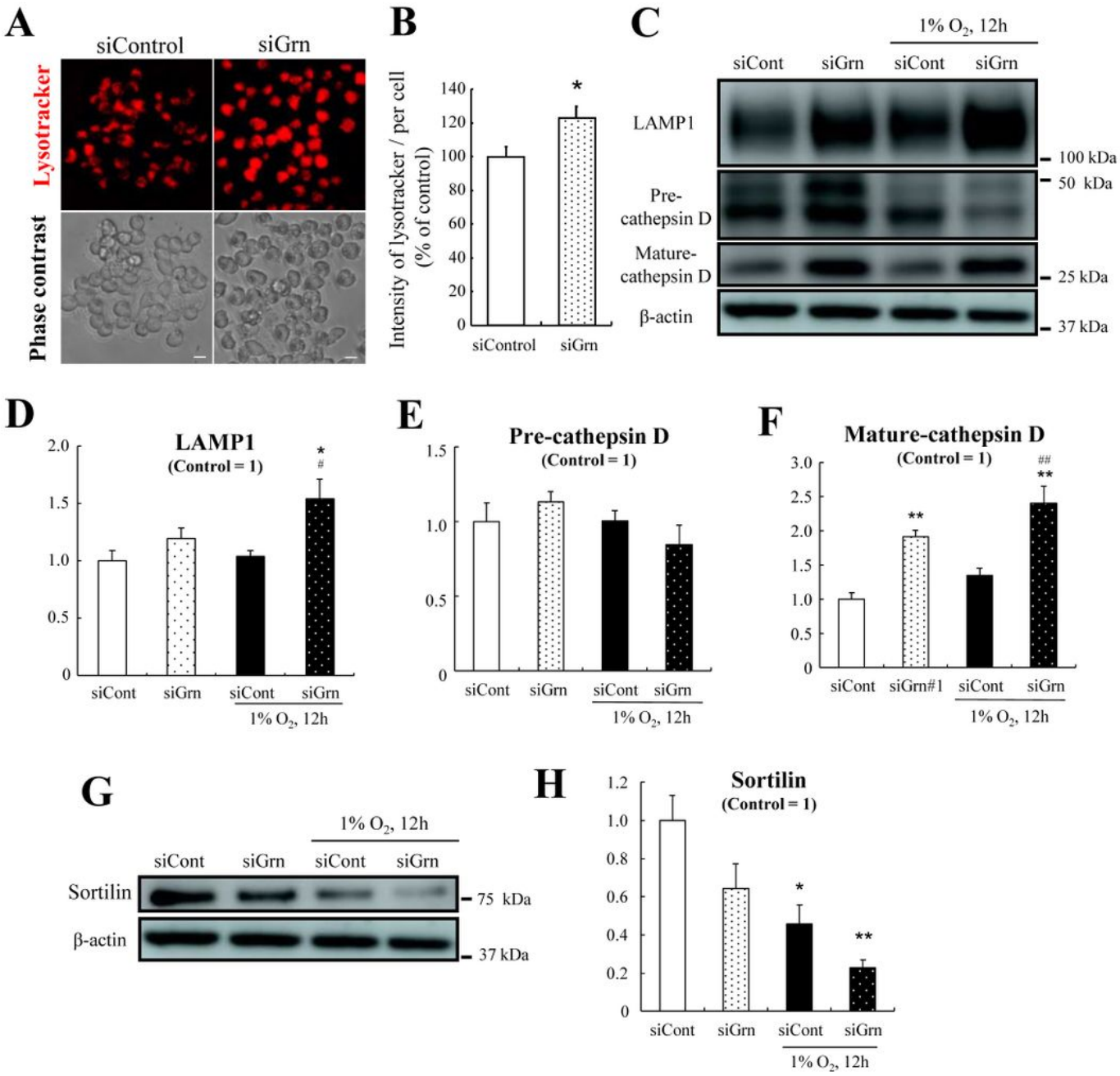


## Figure 6

Lysosomal abnormality in progranulin-silenced macrophages A. Representative images of LysoTracker Red DND-99 staining (red) and phase contrast images of RAW264.7 cells after transfection by siControl or siGrn. Scale bar: 10 μm. B. Quantitative analysis of the fluorescence intensity of LysoTracker+ cells. Data are the means ± SEM (n = 6). *P <0.05 vs. siControl (Welch's t-test). C. Representative images of western blots showing immunoreactivity against LAMP1, cathepsin D, and β-actin. D. E. and F.

Quantitative analysis of expression level of LAMP1 (D), pre-cathepsin D (E), and mature-cathepsin D (F) in RAW264.7 cells after transfection of siControl or siGrn and exposure to hypoxia (1% O2, 12 h). G. and H. Level of expression of sortilin in RAW264.7 cells after transfection by siControl or siGrn and exposure to hypoxia. Data are the means ± SEMs (n = 4). *P <0.05; **P <0.01 vs. siControl; #P <0.05; ##P <0.01 vs. siControl + Hypoxia (one-way ANOVA followed by Tukey's tests).

**Fig. 7**

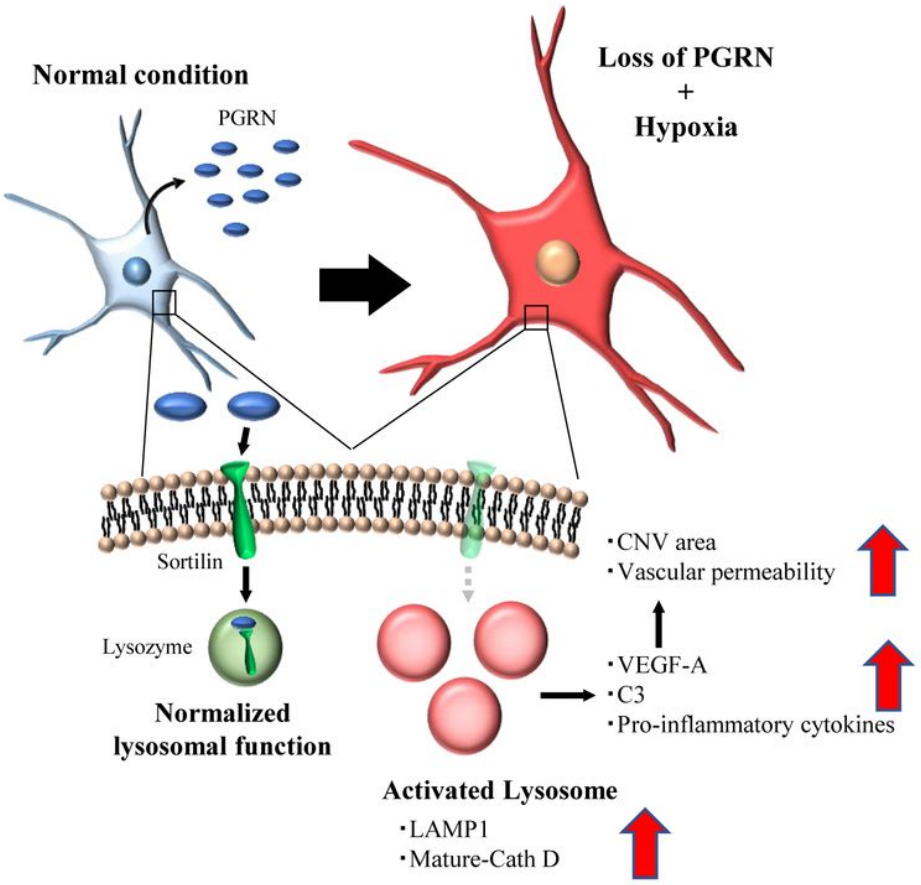


**Figure 7**

Graphical abstract In wild type mice, the myeloid cells including the microglia and macrophages express high levels of PGRN in response to acute inflammation. PGRN regulates the lysosomal function and activation in myeloid cells. However, in PGRN deficient mice, the reduced levels of PGRN lead to abnormal activation of the lysosomes in the myeloid cells. Lysosome activated myeloid cells express proangiogenic and proinflammatory factors and promote formation of CNV and vascular permeability.

## Supplementary Files

This is a list of supplementary files associated with this preprint. Click to download.

- sfig1.jpg
- sfig2.jpg